atmosphere

MDPI

Communication

A New SLF/ELF Algorithm of Fields Excited by a Radiator in a Soil Foundation in the Earth–Ionosphere Cavity

Yuanxin Wang *, Jutao Yang, Shuji Hao, Jing Chen, Yonggan Liang and Yanshuai Zheng

National Key Laboratory of Electromagnetic Environment, China Research Institute of Radiowave Propagation, Qingdao 266107, China; yangjt@crirp.ac.cn (J.Y.); haosj@crirp.ac.cn (S.H.); chenliang@crirp.ac.cn (J.C.); liangyonggan@crirp.ac.cn (Y.L.); zhengyanshuai@crirp.ac.cn (Y.Z.)
* Correspondence: wyx271207@sina.com; Tel.: +86-0532-89078665

Abstract: Abnormal electromagnetic radiation associated with seismic activity has been reported across a wide range of frequencies, but its primary energy is concentrated in the super-low-frequency (SLF) and extremely low-frequency (ELF) bands. To estimate the effect of the seismic radiation source, a radiator in a soil foundation was modeled as a horizontal electric dipole (HED), and the propagation characteristics of the electromagnetic fields were studied in the Earth–ionosphere cavity. The expressions of the electromagnetic fields could be obtained according to the reciprocity theorem. Therefore, a new algorithm named the numerical integral algorithm was proposed, which is suitable for both the SLF and ELF bands. The new algorithm was compared with the asymptotic approximation algorithm when the receiving point was not close to the field source and the antipode. The two algorithms were found to be in excellent agreement, confirming the validity of the new algorithm for SLF and ELF bands.

Keywords: electromagnetic radiation; SLF and ELF; Earth–ionosphere cavity; reciprocity theorem; numerical integral algorithm

Citation: Wang, Y.; Yang, J.; Hao, S.; Chen, J.; Liang, Y.; Zheng, Y. A New SLF/ELF Algorithm of Fields Excited by a Radiator in a Soil Foundation in the Earth–Ionosphere Cavity. *Atmosphere* **2023**, *14*, 1450. https://doi.org/10.3390/atmos14091450

Academic Editor: Christine Amory-Mazaudier

Received: 9 August 2023
Revised: 31 August 2023
Accepted: 6 September 2023
Published: 18 September 2023

1. Introduction

Abnormalities in low-frequency electromagnetic radiation (SLF/ELF) [1,2] have been discovered by earthquake prediction researchers before many earthquakes have occurred. Russian scientists found an earthquake low-frequency abnormality in electromagnetic radiation recorded by a satellite when they analyzed an electromagnetic signal from the Interkosmos-19 satellite in 1983 [3]. A magnetic field abnormality was discovered by the underground low noise observation station Rustrel before an 8.0-magnitude earthquake struck India on 26 January 2001 [4]. Its frequency scope was from 0.03 to 1.0 Hz, and it was 6250 km from the epicenter. An abnormality in ELF electromagnetic radiation was discovered by analyzing ten days of ELF electric and magnetic field data recorded by the French Demeter satellite before a 6.0-magnitude earthquake struck the Adriatic region on 23 November 2004 [5]. Because electromagnetic radiation often appears just before an earthquake occurs, it is an important tool for short-term and imminent earthquake prediction.

Electromagnetic radiation that may be associated with seismic activity has been reported in a wide range of frequencies, but its primary energy is concentrated in the SLF and ELF bands. To further explore this phenomenon and attempt to uncover the rule of earthquake electromagnetic radiation as an indicator of earthquake occurrence, it is imperative that the propagation of such electromagnetic radiation in the SLF and ELF bands [6–8] be studied. To estimate the effect of a seismic source, electromagnetic radiation associated with the seismic activity from a possible seismic current source modeled as an underground HED [9,10] has been studied. However, there is still a need to study the characteristics of electromagnetic fields excited by a radiator in soil foundations in the Earth–ionosphere cavity, with the radiator modeled as an HED [11,12].

According to the International Telecommunication Union (ITU), the frequency range from 30 Hz to 300 Hz is called SLF, and the range below 30 Hz is called ELF. In the SLF and ELF bands, electromagnetic waves can propagate to a distant place along the Earth–ionosphere cavity because the Earth and the ionosphere are both good reflection walls. In ELF frequency bands, the propagation space between the ground and the ionosphere cannot be regarded as a "waveguide [13]", but as a "cavity", because the perimeter of the Earth is comparable to the wavelength.

R.W.P King et al.'s lateral wave propagation theories [14,15] suggest that the electromagnetic field intensity excited by an HED is greater than that excited by a vertical electric dipole (VED) in the SLF and ELF bands. Therefore, a radiator in a soil foundation is idealized as an HED [16–18]. The expressions of electromagnetic fields can be obtained by the VED and the vertical magnetic dipole (VMD) based on the reciprocity theorem. The asymptotic approximation algorithm is suitable for the SLF band, but it is not suitable for the ELF band. Therefore, a new algorithm called the numerical integral algorithm is proposed, which is suitable for the SLF and ELF bands [19–23]. It is compared with the asymptotic approximation algorithm when the receiving point is not close to the field source and the antipode [24]. The propagation characteristic of the fields in the cavity are analyzed and calculated by the numerical integral algorithm in the ELF band.

The paper is arranged into five sections. Section 2 discusses the reciprocity theorem of electromagnetic fields. It is considered as a model. In Section 3, using this model, the expressions of the fields in the Earth–ionosphere cavity are derived. In Section 4, the calculation results are presented and the two algorithms are compared. Section 5 details the conclusions and summarizes the key properties of the electromagnetic fields in the cavity.

2. Fields in the Earth–Ionosphere Cavity

2.1. Reciprocity Theorem of Electromagnetic Fields

Figure 1 shows the reciprocal position of the transmitting antenna, the receiving antenna, and the corresponding system.

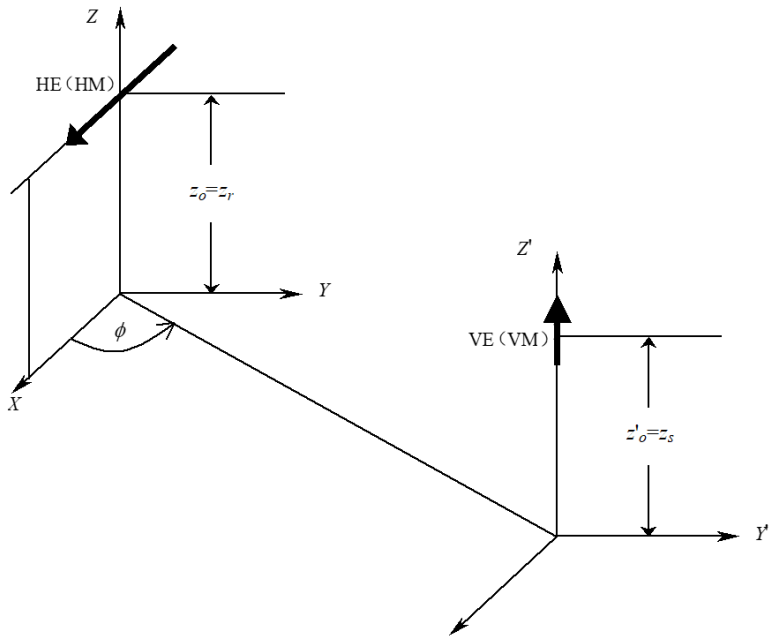

Figure 1. Reciprocal geometry relation of transmitting and receiving antennas.

The voltage V_2 in the second antenna induced by the current I_1 in the first antenna should be equal to the voltage V_1 in the first antenna induced by the current I_2 $(I_1 = I_2)$ in the second antenna, according to the reciprocity theorem.

2.2. Expressions of Fields in the Earth–Ionosphere Cavity

It is assumed that there is a VED in the position of $z'_0 = z_s$ and there is a horizontal electric dipole in the position of $z_0 = z_r$, and its direction parallels the x direction in Figure 1. The voltage in the x direction in the position of z_0 induced by the VED in the position of z_s can be expressed as follows:

$$V^{\mathrm{he}} = -E^{\mathrm{ve}}_{\rho'}(z'_0 = z_s, z_0 = z_r)\cos\varphi\ \mathrm{d}s^{\mathrm{he}} \tag{1}$$

where the superscript characters ve and he represent the vertical and horizontal electric dipoles, respectively, and the subscript character r and s represent the receiving point and the transmitting point, respectively. It is assumed that the current in the transmitting antenna is 1 A. $\mathrm{d}s^{\mathrm{he}}$ is the unit length of the horizontal electric dipole.

The voltage in the position of z_s induced by the horizontal electric dipole in the position of z_0 can be expressed as follows:

$$V^{\mathrm{ve}} = E^{\mathrm{he}}_{z'}(z_0 = z_s, z'_0 = z_r)\mathrm{d}s^{\mathrm{ve}} \tag{2}$$

Equation (1) should be equal to Equation (2) if the lengths of the transmitting antenna and the receiving antenna are the same according to the reciprocity theorem. So, the following can be obtained:

$$E^{\mathrm{he}}_{z'}(z_0 = z_s, z'_0 = z_r) = -E^{\mathrm{ve}}_{\rho'}(z'_0 = z_s, z_0 = z_r)\cos\varphi \tag{3}$$

If the VED is substituted by a vertical magnetic dipole in the position of $z'_0 = z_s$, the voltage in the x direction in the position of z_0 induced by the vertical magnetic dipole can be expressed as follows:

$$V^{\mathrm{he}} = E^{\mathrm{vm}}_{\varphi'}(z'_0 = z_s, z_0 = z_r)\sin\varphi\ \mathrm{d}s^{\mathrm{he}} \tag{4}$$

where the superscript character vm represents the vertical magnetic dipole.

The voltage in the position of z_s induced by the horizontal electric dipole in the position of z_0 can be expressed as follows:

$$V^{\mathrm{vm}} = \mathrm{i}\omega\mu_0 H^{\mathrm{he}}_z(z_0 = z_s, z'_0 = z_r)\mathrm{d}a^{\mathrm{vm}} \tag{5}$$

where $\mathrm{d}a^{\mathrm{vm}}$ is the area of the small current loop.

Equation (4) should be equal to Equation (5) according to the reciprocity theorem. So, the following can be obtained:

$$H^{\mathrm{he}}_z(z_0 = z_s, z'_0 = z_r) = \frac{1}{\mathrm{i}\omega\mu_0}E^{vm}_{\varphi}(z'_0 = z_s, z_0 = z_r)\sin\varphi\frac{\mathrm{d}s^{\mathrm{he}}}{\mathrm{d}a^{\mathrm{vm}}} \tag{6}$$

The expressions of the electromagnetic fields excited by the VED in the Earth–ionosphere cavity are known as follows:

$$E^{ve}_r = -\frac{\mathrm{i}I\mathrm{d}s}{2\omega\varepsilon_0 hr^2}\sum\Lambda^e_n\frac{\nu(\nu+1)}{\sin\nu\pi}F_n(z)F_n(z_0)P_\nu(\cos(\pi-\theta)) \tag{7}$$

$$E^{ve}_\theta = -\frac{\mathrm{i}I\mathrm{d}s}{2\omega\varepsilon_0 hr}\sum\Lambda^e_n\frac{1}{\sin\nu\pi}F_n(z_0)\frac{\mathrm{d}F_n(z)}{\mathrm{d}z}\frac{\partial}{\partial\theta}P_\nu(\cos(\pi-\theta)) \tag{8}$$

$$H^{ve}_\varphi = \frac{I\mathrm{d}s}{2hr}\sum\Lambda^e_n\frac{1}{\sin\nu\pi}F_n(z_0)F_n(z)\frac{\partial}{\partial\theta}P_\nu(\cos(\pi-\theta)) \tag{9}$$

where

$$\Lambda^e_n = \frac{1}{1+\frac{\sin 2kC_n h}{2kC_n h}},\ \nu(\nu+1) = k^2a^2S^2_n,\ S_n = \sqrt{1-C^2_n},$$

$F_n(z)$ is the height function of n modes. $P_\nu(\cos(\pi-\theta))$ is the Legendre function.

$$F_n(z) = \frac{1}{1+R_g}\{\exp[-\mathrm{i}k\int_0^z (C_n^2 + \frac{2tS_n^2}{a})^{\frac{1}{2}}\mathrm{d}t] + R_g\exp[\mathrm{i}k\int_0^z (C_n^2 + \frac{2t}{a}S_n^2)^{\frac{1}{2}}\mathrm{d}t]\}$$

where C_n can be obtained by the following mode function.

$$R_i R_g \exp(2\mathrm{i}kC_n h) = \mathrm{e}^{2\mathrm{i}n\pi} \tag{10}$$

where

$$R_g = \frac{C_n - \Delta_g}{C_n + \Delta_g},\ R_i = \frac{C_n - \Delta_i}{C_n + \Delta_i}$$

In the spherical coordinate system, by substituting (8) into (3), the following can be obtained:

$$E_r^{\mathrm{he}}(r,\theta,\varphi) = -\frac{\mathrm{i}I\mathrm{d}s^{\mathrm{he}}\eta\cos\varphi}{2ha}\frac{\partial P_\nu(\cos(\pi-\theta))}{\sin\nu\pi\partial\theta}\sum_{n=0}^{\infty}\Lambda_n^e F_n(z_r)\frac{\partial F_n(z_s)}{k\partial z} \tag{11}$$

The expressions of the electromagnetic fields excited by the vertical magnetic dipole in the Earth–ionosphere cavity are known as follows:

$$E_\varphi^{vm} = \frac{\mathrm{i}\omega\mu_0 I\mathrm{d}a}{4r}\frac{\partial}{\partial\theta}P_\nu(\cos(\pi-\theta))\sum_m \frac{G_m^h(z_s)}{\sin(\mu\pi)N_m}G_m^h(z_r) \tag{12}$$

$$H_r^{vm} = -\frac{I\mathrm{d}a}{4r^2}P_\nu(\cos(\pi-\theta))\sum_m \frac{\nu(\nu+1)}{\sin(\mu\pi)N_m}G_m^h(z_s)G_m^h(z_r) \tag{13}$$

$$H_\theta^{vm} = -\frac{I\mathrm{d}a}{4r}\frac{\partial}{\partial\theta}P_\nu(\cos(\pi-\theta))\sum_m \frac{G_m^h(z_s)}{\sin(\mu\pi)N_m}\frac{\partial}{\partial z}G_m^h(z_r) \tag{14}$$

where

$$N_m = -\frac{h}{2\Delta_g^2 C_m^2}[1 - \frac{\sin 2kC_m h}{2kC_m h} - \Delta_g^2 C_m^2(1 + \frac{\sin 2kC_m h}{2kC_m h}) - \mathrm{i}\frac{\Delta_g}{kh}(\cos 2kC_m h - 1)]$$

$$G_m^h(z) = \{\exp[-\mathrm{i}k\int_0^z (C_m^2 + \tfrac{2t}{a}S_m^2)^{1/2}\mathrm{d}t] + R_g^h\exp[\mathrm{i}k\int_0^z (C_m^2 + \tfrac{2t}{a}S_m^2)^{1/2}\mathrm{d}t]\}(1+R_g^h)^{-1}$$

where C_m can be obtained by the following mode function:

$$R_g^h R_i^h \exp[2\mathrm{i}k\int_0^h (C_m^2 + \frac{2t}{a}S_n^2)^{1/2}\mathrm{d}t] = \mathrm{e}^{2\mathrm{i}(m-1)\pi} \tag{15}$$

where

$$R_g^h = (C_m - \Delta_g^{-1})(C_m + \Delta_g^{-1})^{-1},\ R_i^h = (C'_m - \Delta_i^{-1})(C'_m + \Delta_i^{-1})^{-1},\ C'_m = (C_m^2 + \frac{2h}{a}S_m^2)^{1/2} \approx C_m$$

By substituting (12) into (6), the following can be obtained:

$$H_r^{\mathrm{he}}(r,\theta,\varphi) = \frac{I\mathrm{d}s^{\mathrm{he}}}{2ha}\sin\varphi\frac{\partial P_\nu[\cos(\pi-\theta)]}{\sin\mu\pi\partial\theta}\sum_m \Lambda_m^h G_m^h(z_r)G_m^h(z_s) \tag{16}$$

where

$$\Lambda_m^h = \Delta_g^2 C_m^2[1 - \frac{\sin 2kC_m h}{2kC_m h} - \Delta_g^2 C_m^2\ (1 + \frac{\sin 2kC_m h}{2kC_m h}) - \mathrm{i}\frac{\Delta_g}{kh}(\cos 2kC_m h - 1)]^{-1}$$

It can be obtained by the Maxwell function.

$$\frac{1}{r\sin\theta}[\frac{\partial}{\partial\theta}\sin\theta H_\varphi - \frac{\partial H_\theta}{\partial\varphi}] = -\mathrm{i}\omega\varepsilon_0 E_r \tag{17}$$

$$\frac{1}{r}[\frac{1}{\sin\theta}\frac{\partial H_r}{\partial\varphi} - \frac{\partial}{\partial r}(rH_\varphi)] = -\mathrm{i}\omega\varepsilon_0 E_\theta \tag{18}$$

$$\frac{1}{r}[\frac{\partial}{\partial r}(rH_\theta) - \frac{\partial H_r}{\partial\theta}] = -\mathrm{i}\omega\varepsilon_0 E_\varphi \tag{19}$$

$$\frac{1}{r\sin\theta}[\frac{\partial}{\partial\theta}\sin\theta E_\varphi - \frac{\partial E_\theta}{\partial\varphi}] = \mathrm{i}\omega\mu_0 H_r \tag{20}$$

$$\frac{1}{r}[\frac{1}{\sin\theta}\frac{\partial E_r}{\partial\varphi} - \frac{\partial}{\partial r}(rE_\varphi)] = \mathrm{i}\omega\mu_0 H_\theta \tag{21}$$

$$\frac{1}{r}[\frac{\partial}{\partial r}(rE_\theta) - \frac{\partial E_r}{\partial\theta}] = \mathrm{i}\omega\mu_0 H_\varphi \tag{22}$$

By substituting (11) and (16) into (17)~(22), the expressions of the electromagnetic fields can be obtained, such as

$$E_r^{\mathrm{he}}(a,\theta,\varphi) = -\frac{I\mathrm{d}s\eta\Delta_{gs}}{2ha}\cos\varphi\frac{\partial P_\nu(\cos(\pi-\theta))}{\sin\nu\pi\partial\theta}\sum_n \Lambda_n^e \tag{23}$$

$$E_\theta^{\mathrm{he}}(a,\theta,\varphi) = -\frac{\mathrm{i}I\mathrm{d}s\eta}{2ha}\cos\varphi\{-\frac{\Delta_{gs}\Delta_{gr}}{ka}\frac{\partial^2 P_\nu(\cos(\pi-\theta))}{\sin\nu\pi\partial\theta^2}\sum_n \Lambda_n^e S_n^{-2} - \frac{1}{ka\sin\theta}\frac{\partial P_v(\cos(\pi-\theta))}{\sin v\pi\partial\theta}\sum_m \Lambda_m^h S_m^{-2}\} \tag{24}$$

$$H_\varphi^{\mathrm{he}}(a,\theta,\varphi) = \frac{I\mathrm{d}s}{2ha}\cos\varphi[-\frac{\mathrm{i}\Delta_{gs}}{ka}\frac{\partial^2 P_v(\cos(\pi-\theta))}{\sin v\pi\partial\theta^2}\sum_n \Lambda_n^e S_n^{-2} - \frac{\mathrm{i}}{ka\sin\theta\Delta_{gr}}\frac{\partial P_v(\cos(\pi-\theta))}{\sin v\pi\partial\theta}\sum_m \Lambda_m^h S_m^{-2}] \tag{25}$$

where Δ_{gs} is the surface impedance in the position of the transmitting antenna, and Δ_{gr} is the surface impedance in the position of the receiving antenna.

3. Algorithms of the Legendre Function and Its Differential Coefficient

3.1. Asymptotic Approximation Algorithm

When $ka >> 1$, and the observation point is not close to the field source and the antipode, the following can be obtained:

$$\frac{P_\nu[\cos(\pi-\theta)]}{\sin\nu\pi} \approx -\sqrt{\frac{2}{\pi(\nu+0.5)\sin\theta}}\exp[\mathrm{i}(\nu+0.5)\theta + \mathrm{i}\frac{\pi}{4}] \approx -\sqrt{2}(\pi kaS_n\sin\theta)^{-1/2}\exp(\mathrm{i}kaS_n\theta + \mathrm{i}\pi/4) \tag{26a}$$

So, the following Formula (26b) can be obtained by taking the partial derivative of Formula (26a).

$$\frac{\partial P_\nu(\cos(\pi-\theta))}{\sin\nu\pi\partial\theta} \approx -\mathrm{i}\sqrt{\frac{2kaS_n}{\pi\sin\theta}}\exp(\mathrm{i}kaS_n\theta + \mathrm{i}\frac{\pi}{4}) \tag{26b}$$

and

$$\frac{\partial^2 P_\nu(\cos(\pi-\theta))}{\sin\nu\pi\partial^2\theta} \approx \sqrt{\frac{2}{\pi\sin\theta}}(kaS_n)^{3/2}\exp(\mathrm{i}kaS_n\theta + \mathrm{i}\frac{\pi}{4}) \tag{27}$$

When it is close to the antipode, δ is equal to $\pi-\theta$, and δ is very small, so the Legendre functions may be approximately obtained

$$\begin{aligned} &P_\nu[\cos(\pi-\theta)] = (1+\tfrac{\delta^2}{12})J_0(x) - \tfrac{\delta}{24(\nu+0.5)}J_1(x) \\ &\tfrac{\partial}{\partial\theta}P_\nu(\cos(\pi-\theta)) \approx -\tfrac{\delta}{8}J_0(x) + (\nu+\tfrac{1}{2})(1+\tfrac{\delta^2}{12})J_1(x) \\ &\tfrac{\partial^2 P_\nu(\cos(\pi-\theta))}{\partial^2\theta} \approx -[(\nu+0.5)^2(1+\tfrac{\delta^2}{12}) - \tfrac{1}{8}]J_0(x) + \tfrac{\nu+0.5}{\delta}J_1(x)(1-\tfrac{\delta^2}{24}) + \cdots \\ &\qquad\qquad \approx -\tfrac{1}{2}[(\nu+0.5)^2 - \tfrac{1}{4}] + \tfrac{3\delta^2}{16}(\nu+0.5)^2[(\nu+0.5)^2 - \tfrac{7}{6}] + \cdots \end{aligned} \tag{28}$$

When it is close to the field source and $\theta << 1$, the following can be obtained:

$$\begin{aligned} &\tfrac{P_\nu(\cos(\pi-\theta))}{\sin\nu\pi} \approx -\mathrm{i}H_0^{(1)}((\nu+0.5)\theta) \\ &\tfrac{\partial P_\nu(\cos(\pi-\theta))}{\sin\nu\pi\partial\theta} \approx \mathrm{i}(\nu+0.5)(1+\tfrac{\theta^2}{12})H_1^{(1)}((\nu+0.5)\theta) \approx \mathrm{i}(\nu+0.5)H_1^{(1)}((\nu+0.5)\theta) \\ &\tfrac{\partial^2 P_\nu(\cos(\pi-\theta))}{\sin\nu\pi\partial^2\theta} \approx -\tfrac{\mathrm{i}(\nu+0.5)H_1^{(1)}((\nu+0.5)\theta)}{\theta} \end{aligned} \tag{29}$$

3.2. Numerical Integral Algorithm

The asymptotic approximation algorithm is only used when $ka >> 1$. So, it cannot be used in the ELF band because $ka >> 1$ is not satisfied in the ELF band. In order to find a new algorithm to be used in the SLF and ELF bands, a numerical integral algorithm is proposed [25].

$$P_v(\cos\theta) = \frac{2}{\pi}\int_0^\theta \frac{\cos[(v+0.5)t]}{\sqrt{2(\cos t - \cos\theta)}}dt \tag{30}$$

So

$$P_v[\cos(\pi-\theta)] = \frac{2}{\pi}\int_0^{\pi-\theta} \frac{\cos[(v+0.5)t]}{\sqrt{2[\cos t - \cos(\pi-\theta)]}}dt \tag{31}$$

It is divided into two parts because the denominator is equal to zero in Equation (31) when t is equal to $\pi-\theta$.

$$P_v[\cos(\pi-\theta)] = I_1 + I_2 \tag{32}$$

where

$$I_1 = \frac{2}{\pi}\int_0^{\pi-\theta-\delta} \frac{\cos[(v+0.5)t]}{\sqrt{2[\cos t - \cos(\pi-\theta)]}}dt,\ I_2 = \frac{2}{\pi}\int_{\pi-\theta-\delta}^{\pi-\theta} \frac{\cos[(v+0.5)t]}{\sqrt{2[\cos t - \cos(\pi-\theta)]}}dt$$

I_1 may be calculated by the Simpson numerical integral formula. So, the following can be obtained:

$$I_1 = \frac{\pi-\theta-\delta}{3\pi}\left\{\frac{1}{\sqrt{2[1-\cos(\pi-\theta)]}} + 4\frac{\cos[(v+0.5)(\pi-\theta-\delta)/2]}{\sqrt{2\{\cos[(\pi-\theta-\delta)/2] - \cos(\pi-\theta)\}}} + \frac{\cos[(v+0.5)(\pi-\theta-\delta)]}{\sqrt{2[\cos(\pi-\theta-\delta) - \cos(\pi-\theta)]}}\right\} \tag{33}$$

If it is assumed that $\pi-\theta-l=t$, I_2 may be rewritten as follows:

$$I_2 = \frac{1}{\pi}\int_0^\delta \frac{\cos[(v+0.5)(\pi-\theta-l)]}{\sqrt{\sin(\pi-\theta-l/2)\sin l/2}}dl \tag{34}$$

when $\delta \to 0$, I_2 may be changed as follows:

$$\begin{aligned} I_2 &= \tfrac{1}{\pi}\left\{\tfrac{\cos[(v+0.5)(\pi-\theta-\delta)]}{\sqrt{\sin(\pi-\theta-\delta/2)}} - \tfrac{\cos[(v+0.5)(\pi-\theta)]}{\sqrt{\sin(\pi-\theta)}}\right\}\int_0^\delta \sqrt{\tfrac{2}{l}}dl \\ &= \tfrac{2\sqrt{2\delta}}{\pi}\left\{\tfrac{\cos[(v+0.5)(\pi-\theta-\delta)]}{\sqrt{\sin(\pi-\theta-\delta/2)}} - \tfrac{\cos[(v+0.5)(\pi-\theta)]}{\sqrt{\sin(\pi-\theta)}}\right\} \end{aligned} \tag{35}$$

because

$$P'_v(z) = \frac{v}{z^2-1}[zP_v(z) - P_{v-1}(z)] \tag{36}$$

$$P''_v(z) = \frac{v}{(z^2-1)^2}\left\{\left[z^2(v-1)-1\right]P_v(z) - z(2v-3)P_{v-1}(z) + (v-1)P_{v-2}(z)\right\} \tag{37}$$

The following can be obtained:

$$\begin{array}{l} \frac{\partial P_v[\cos(\pi-\theta)]}{\partial\theta} = -\frac{v}{\sin(\pi-\theta)}\{\cos(\pi-\theta)P_v[\cos(\pi-\theta)] - P_{v-1}[\cos(\pi-\theta)]\} \\ \frac{\partial^2 P_v[\cos(\pi-\theta)]}{\partial^2\theta} = \frac{v}{\sin^3(\pi-\theta)}\{[(v-1)\cos^2(\pi-\theta)-1]P_v[\cos(\pi-\theta)] - (2v-3)\cos(\pi-\theta)P_{v-1}[\cos(\pi-\theta)] + (v-1)P_{v-2}[\cos(\pi-\theta)]\} \end{array} \tag{38}$$

4. Calculation Results and Discussion

The calculation results were obtained under the nonideal electric conductor condition. In this case, the altitude of the low ionosphere was taken as h = 70 km during the day. The radius of the Earth was a = 6370 km. The conductivity of the ground was $\sigma_g = 10^{-4}$ s/m, and the conductivity of the ionosphere was $\sigma_i = 10^{-5}$ s/m. The current moment of the electric dipole was $Idl = 1$ Am.

Figure 2 shows the variation in the electric field component E_r along the propagation distance, where the solid line represents the result calculated by the asymptotic approximation algorithm, and the dashed line represents the result calculated by the numerical integral algorithm. The calculations are both under the condition that the dipole is located 5 m in the soil foundation, and the receiving point is located on the surface of the Earth, which is not close to the field source and the antipode, and the frequency is f = 100 Hz, and $\varphi = \pi/4$.

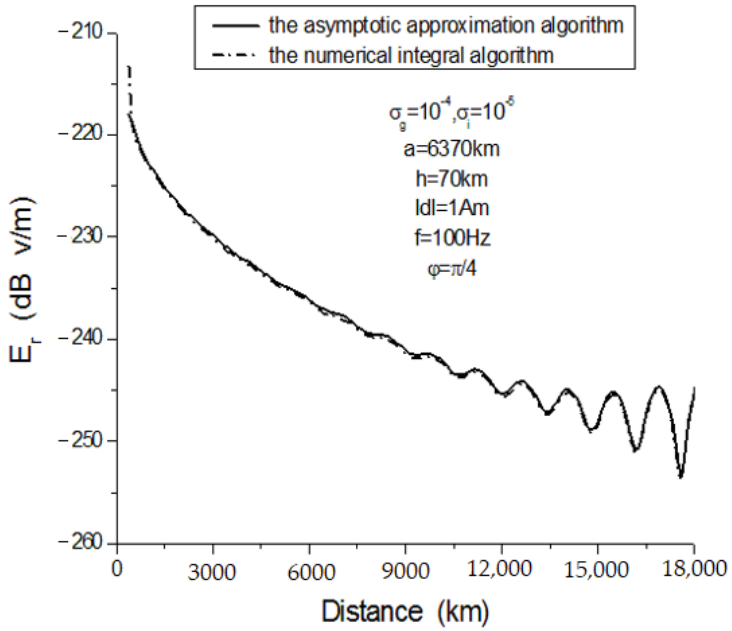

Figure 2. Variation in the electric field component E_r along the propagation distance.

It can be seen from Figure 2 that the two algorithms agree well. It can be clearly seen that they can correctly show the "interference" phenomenon of two waves' propagation along the short great-circle way and the long great-circle way when they pass through the antipode to the receiver after 10,000 km, because the attenuation ratio of the SLF wave propagation in the cavity is very small. The "interference" phenomenon is more and more evident after 10,000 km.

Figure 3 shows the variation in the electromagnetic field components along the propagation distance near the antipode, which is calculated by the numerical integral algorithm.

The calculations are both under the condition that the dipole is located 5 m in the soil foundation, the receiving point is located on the surface of the Earth, and the frequency is f = 100 Hz, and $\varphi = \pi/4$.

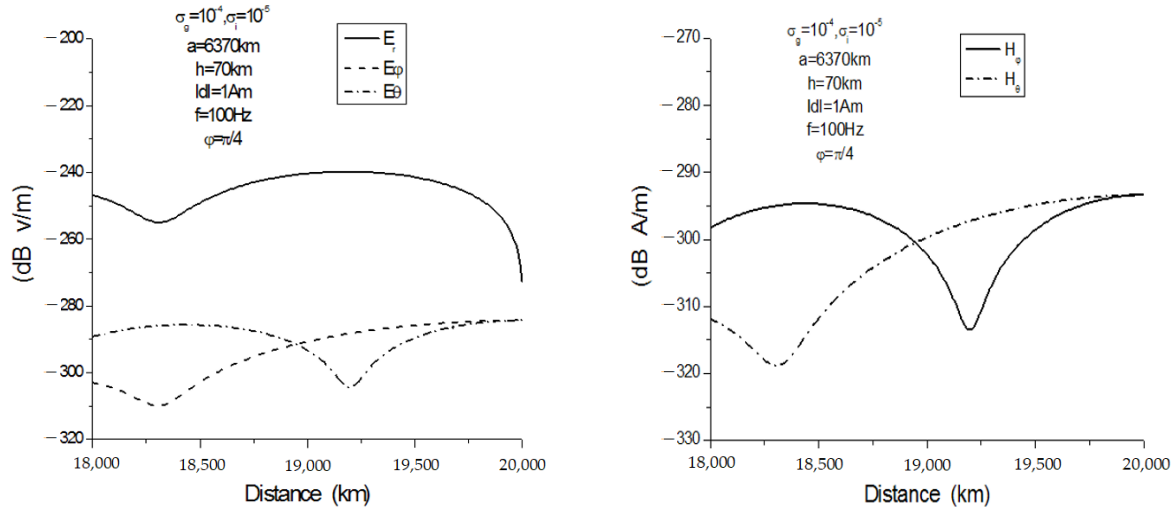

(**a**) (**b**)

Figure 3. Variation in the electromagnetic field components along the distance from antipode. (**a**) electric field component; (**b**) magnetic field component.

It can be seen from Figure 3 that the variation rules of the electric field component E_θ and the magnetic field component H_φ are just the same, and the value of the electric field component E_θ is larger than that of the magnetic field component H_φ. The variation rules of the electric field component E_φ and the magnetic field component H_θ are just the same, and the value of the electric field component E_φ is larger than that of the magnetic field component H_θ. The value of the electric field component E_r is the largest. The "interference" phenomenon of two waves' propagation along the short great-circle way and the long great-circle way when they pass through the antipode to the receiver can be clearly seen, because the attenuation ratio of the SLF wave propagation in the cavity is very small.

Figure 4 shows the variation in the electric field component E_r along the propagation distance, which is calculated by the numerical integral algorithm. The calculations are both under the condition that the dipole is located 5 m in the soil foundation, the receiving point is located on the surface of the Earth, and the frequency is f = 8 Hz, f = 15 Hz, f = 20 Hz, f = 30 Hz, and $\varphi = \pi/4$.

It can be seen in Figure 4 that different-colored line segments are used to represent the different frequencies. Their wavelength is less than half of the perimeter of the Earth when the frequencies are equal to 15 Hz, 20 Hz, and 30 Hz. The "interference" phenomena of two waves' propagation along the short great-circle way and the long great-circle way are more and more evident when they pass through the antipode to the receiver, because the attenuation ratio of the SLF wave propagation in the cavity is very small. The values of the electric field component E_r become more and more small along the propagation distance. The "interference" phenomena become more and more obvious with the increase in the frequency. The wavelength is almost equal to the perimeter of the Earth when the frequency is equal to 8 Hz. The fields in the cavity are a kind of "standing wave", and the "interference" phenomenon already disappears.

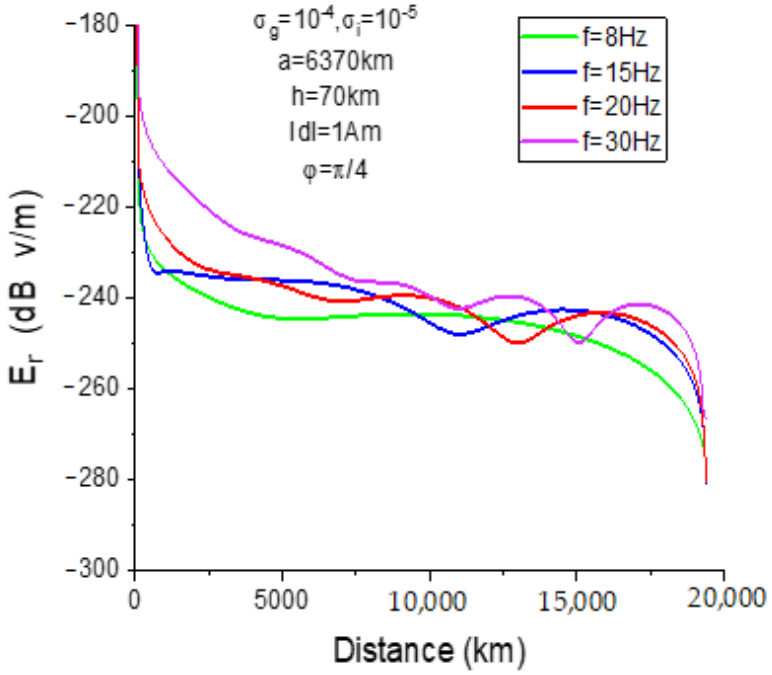

Figure 4. Variation in the electric field component E_r along the propagation distance with different frequency.

5. Conclusions

In order to estimate the effect of a seismic source, the characteristic of the electromagnetic fields excited by a radiator in a soil foundation in the Earth–ionosphere cavity still needs to be studied, with the radiator modeled as an HED. Its expressions of the electromagnetic fields can be obtained by the expressions of the electromagnetic fields excited by a VED and VMD according to the reciprocity theorem. The asymptotic approximation algorithm is suitable for the SLF band, but it is not suitable for the ELF band. Therefore, the numerical integral algorithm is proposed, which is suitable for the SLF and ELF bands. It is compared with the asymptotic approximation algorithm when the receiving point is not close to the field source and the antipode, and their results agree well. Therefore, the new algorithm is correct. The characteristic of the electromagnetic fields in the cavity is analyzed and calculated by the numerical integral algorithm in the ELF band.

Author Contributions: Conceptualization, Y.W. and J.Y.; writing—original draft preparation, Y.W., J.Y. and J.C.; writing—review and editing, Y.L., J.C. and Y.Z.; supervision, S.H. All authors have read and agreed to the published version of the manuscript.

Funding: This work was supported by the Foundation of the National Key Laboratory of Electromagnetic Environment of China [Grant No. JCKY2023210C614240302].

Institutional Review Board Statement: Not applicable.

Informed Consent Statement: Not applicable.

Data Availability Statement: Data set available on request to corresponding authors.

Acknowledgments: We are deeply grateful to the anonymous reviewers for their constructive comments. I would like to thank all who have contributed to this paper.

Conflicts of Interest: The authors declare no conflict of interest.

References

1. Mavromatis, F.; Boursianis, A.; Samaras, T.; Koukourlis, C.; Sahalos, J.N. A broadband monitoring system for electromagnetic-radiation assessment. *IEEE Antennas Propag. Mag.* **2009**, *51*, 71–79. [CrossRef]
2. Hisatoshi, B. Investigation of electromagnetic radiation associated with earthquakes observational results related to earthquakes. *Tokai Daigaku Sogo Kagaku Gijutsu Kenkyujo Kenkyukai Shiryoshu* **2000**, *19*, 67–74.

3. Larkina, V.I.; Nalivayko, A.V.; Gerhenzon, N.I.; Gokhberg, M.B.; Liperovskiy, V.A.; Shalimov, S.L. Observations of VLF emissions related with seismic activity, on the Interkosmos-19 satellite. *Geomagn. Aeron.* **1983**, *23*, 684–687.
4. Gaffet, S.; Guglielmi, Y.; Virieux, J.; Waysand, G.; Chwala, A.; Stolz, R.; Emblanch, C.; Auguste, M.; Boyer, D.; Cavaillou, A. Simultaneous seismic and magnetic measurements in the Low-Noise underground laboratory (LSBB) of Rustrel, France, during the 2001 January 26 Indian earthquake. *Geophys. J. Int.* **2003**, *155*, 981–990. [CrossRef]
5. Boudjada, M.Y.; Schwingenschuh, K.; Biernat, H.K.; Berthelier, J.J.; Blecki, J.; Parrot, M.; Stachel, M.; Aydogar, Ö.; Stangl, G.; Weingrill, J. Similar behaviors of natural ELF/VLF ionospheric emissions and transmitter signals over seismic Adriatic regions. *Nat. Hazards Earth Syst. Sci.* **2008**, *8*, 1229–1236. [CrossRef]
6. Pan, W.Y. *Long Wave beyond Long Wave Extremely Long Wave Propagation*; Electric Scientific and Technical University Press: Chengdu, China, 2004; pp. 343–350.
7. Bannister, P. Far-field Extremely Low Frequency (ELF) propagation measurements, 1970–1972. *IEEE Trans. Commun.* **1974**, *22*, 468–474. [CrossRef]
8. Galejs, J. *Terrestrial Propagation of Long Electromagnetic Wave*; Pergamon Press: Oxford, UK, 1972; pp. 87–96.
9. Wang, Y.-X.; Jin, R.-H.; Geng, J.-P.; Liang, X.-L. Exact SLF/ELF underground HED field strengths in earth-ionosphere cavity and Schumann Resonance. *IEEE Trans. Antennas Propag.* **2011**, *59*, 3031–3039. [CrossRef]
10. Wang, Y.-X.; Jin, R.-H.; Geng, J.-P.; Liang, X.-L. Propagation of SLF/ELF electromagnetic waves excited by an underground HED in the lower ionosphere. *IEEE Trans. Antennas Propag.* **2012**, *60*, 5412–5418. [CrossRef]
11. Bannister, P. Some notes on ELF earth-ionosphere waveguide daytime propagation parameters. *IEEE Trans. Antennas Propag.* **1979**, *27*, 696–698. [CrossRef]
12. Tripathi, V.K.; Chang, C.L.; Papadopoulos, K. Excitation of the Earth-ionosphere waveguide by an ELF source in the ionosphere. *Radio Sci.* **1982**, *17*, 1321–1326. [CrossRef]
13. Cummers, S.A. Modeling electromagnetic propagation in the Earth-ionosphere waveguide. *IEEE Trans. Antennas Propag.* **2000**, *48*, 1420–1429. [CrossRef]
14. King, R.W.P.; Owens, M.; Wu, T.T. *Lateral Electromagnetic Wave*; Springer: Berlin, Germany, 1992; pp. 134–152.
15. Wait, J.R. *Electromagntic Waves in Stratified Media*; IEEE: New York, NY, USA, 1962; pp. 126–138.
16. Li, K.; Lu, Y.; Li, M. Approximate formulas for lateral electromagnetic pulses from a horizontal electric dipole on the surface of one-dimensionally anisotropic medium. *IEEE Trans. Antennas Propag.* **2005**, *53*, 933–937.
17. Barrick, D.E. Exact ULF/ELF dipole field strengths in the Earth-ionosphere cavity over the Schumann resonance region: Idealized boundaries. *Radio Sci.* **1999**, *34*, 209–227.
18. Wang, Y.-X.; Jin, R.-H.; Geng, J.-P. Fast convergence algorithm for earthquake prediction using SLF/ELF HED during day and night and Schumann resonance. *Wirel. Pers. Commun.* **2012**, *67*, 149–163. [CrossRef]
19. Dong, H.; Yan, Y.-B.; Li, Q.-L. FDTD analysis of fields excited by horizontal electric dipole in asymmetric earth-ionosphere cavity. *Chin. J. Radio Sci.* **2010**, *25*, 276–280.
20. Soriano, A.; Navarro, E.A.; Paul, D.L.; Porti, J.A.; Morente, J.A.; Craddock, I.J. Finite difference time domain simulation of the earth-ionosphere resonant cavity: Schumann Resonance. *IEEE Trans. Antennas Propag.* **2005**, *53*, 1535–1541. [CrossRef]
21. Simpson, J.J.; Taflove, A. Three-dimensional FDTD modeling of impulsive ELF antipodal propagation and Schumann resonance of the Earth-sphere. *IEEE Trans. Antennas Propag.* **2004**, *52*, 443–451. [CrossRef]
22. Otsuyama, T.; Sakuma, D.; Hayakawa, M. FDTD analysis of ELF wave propagation and Schumann resonance for a subionosphere waveguide model. *Radio Sci.* **2003**, *38*, 1103. [CrossRef]
23. Simpson, J.J. Global FDTD Maxwell's Equations Modeling of Electromagnetic Propagation From Currents in the Lithosphere. *IEEE Trans. Antennas Propag.* **2008**, *56*, 199–203. [CrossRef]
24. Fraser-Smith, A.C.; Bannister, P.R. Reception of ELF signals at antipodal distances. *Radio Sci.* **1998**, *33*, 83–88. [CrossRef]
25. Jeffrey, A. *Table of Integrals, Series, and Products*; Academic Press: New York, NY, USA, 1980; pp. 256–269.